frontiers in Materials

ORIGINAL RESEARCH
published: 09 July 2019
doi: 10.3389/fmats.2019.00163

# Synthesis of $Cr_2O_3$ Nanoparticle-Coated $SnO_2$ Nanofibers and $C_2H_2$ Sensing Properties

*Xin Gao [1], Qu Zhou [1,2]*, Zhaorui Lu [1], Lingna Xu [1], Qingyan Zhang [1] and Wen Zeng [3]*

[1] College of Engineering and Technology, Southwest University, Chongqing, China, [2] Electrical and Computer Engineering Department, Wayne State University, Detroit, MI, United States, [3] College of Materials Science and Engineering, Chongqing University, Chongqing, China

In this work, $Cr_2O_3$ nanoparticles, and $SnO_2$ nanofibers were fabricated by a sol–gel process and an electrospinning method, respectively. Gas sensitive materials with high sensitivity to $C_2H_2$ gas were obtained by coating $Cr_2O_3$ nanoparticles on $SnO_2$ nanofibers. The prepared $Cr_2O_3$ nanoparticle-coated $SnO_2$ nanofibers ($Cr_2O_3$ NPs. coated $SnO_2$ NFs.) were characterized by X-ray diffraction (XRD), scanning electron microscope (SEM), X-ray energy dispersive spectroscopy (EDS), X-ray photoelectron spectroscopy (XPS), and the gas sensing behaviors to $C_2H_2$ were studied. The $Cr_2O_3$ NPs. coated $SnO_2$ NFs. exhibited low optimal operating temperature, high sensing response, excellent response-recovery time, and long-term stability to $C_2H_2$. The optimal operating temperature of the measured material to 20 ppm $C_2H_2$ was about 220°C and the $C_2H_2$ concentration had a good linear relationship with the response value when the concentration was 60 ppm. In addition, a reasonable gas sensing mechanism was proposed which may enhance the gas sensing performances for the $Cr_2O_3$ NPs. coated $SnO_2$ NFs. to $C_2H_2$.

**Keywords: $Cr_2O_3$ nanoparticles, $SnO_2$ nanofibers, electrospinning, $C_2H_2$, sensing properties**

OPEN ACCESS

***Edited by:***
*Zhenyu Li,*
*Southwest Petroleum University, China*

***Reviewed by:***
*Qi Qi,*
*Jilin University, China*
*Yingming Xu,*
*Heilongjiang University, China*

***Correspondence:***
*Qu Zhou*
*zhouqu@swu.edu.cn*

***Specialty section:***
*This article was submitted to Functional Ceramics, a section of the journal Frontiers in Materials*

***Received:*** *19 May 2019*
***Accepted:*** *24 June 2019*
***Published:*** *09 July 2019*

***Citation:***
*Gao X, Zhou Q, Lu Z, Xu L, Zhang Q and Zeng W (2019) Synthesis of $Cr_2O_3$ Nanoparticle-Coated $SnO_2$ Nanofibers and $C_2H_2$ Sensing Properties. Front. Mater. 6:163. doi: 10.3389/fmats.2019.00163*

## INTRODUCTION

Metal oxide semiconductors have important practical significance in gas sensing, mainly because of good chemical reliability, real-time monitoring, and easy fabrication (Zhou et al., 2018b; Wei et al., 2019b). The basis of functional materials, including ZnO (Wang et al., 2019; Yoo et al., 2019), $TiO_2$ (Crişan et al., 2018; Meng et al., 2019), $In_2O_3$ (Liu et al., 2018; Inyawilert et al., 2019), $SnO_2$ (Zhang et al., 2018; Zhou et al., 2018c; Li et al., 2019a), have been applied in gas sensing in the past for a long time. Among them, $SnO_2$ is one of the earliest metal oxides, due to its wide band gap, excellent physicochemical properties, and low-price for gas sensing (Uddin and Chung, 2015; Thanihaichelvan et al., 2019). It can easily generate oxygen vacancies on the surface, leading to high specific surface area, and excellent sensing properties (Zhang et al., 2017; Ren et al., 2019). For $SnO_2$, various morphologies of nanostructures have been reported, for instance, zero dimensional nanoparticles (Ahmed et al., 2019), one dimensional nanorods (Zhou et al., 2016), nanowires (Tonezzer, 2019), and nanofibers (Mudra et al., 2019), and two dimensional nanosheets

(Chang et al., 2019). Among them, one dimensional nanostructures have been rapidly developed due to their surprising properties such as easy control dimension, large surface area to volume ratio, and excellent mechanical performance (Wang et al., 2017b; Bai et al., 2018).

In order to improve the sensitivity of pure $SnO_2$ nanofibers for gas detection more effectively, several approaches have been studied such as the addition of catalysts, doping metals, and metal oxides (Lu et al., 2018; Zhou et al., 2018d; Zheng et al., 2019). Various studies on gas sensing properties of $SnO_2$ nanofibers doped or coated with metal or metal oxide have been reported so far. Qi et al. reported $Sm_2O_3$-doped $SnO_2$ showed high sensitivity under various humidity conditions to $C_2H_2$ (Qi et al., 2008). Li et al. confirmed the sensor made of $La^{3+}$ doped $SnO_2$ nanofibers could rapidly correspond to hydrogen, with good selectivity, and long-range linear response (Li et al., 2019b). Chromium is a very interesting dopant because of its unique catalytic properties and several stable valence states. In addition, it can be used to adjust the surface states, energy band gap and carrier transport characteristics of semiconductors. Gönüllü et al. investigated Cr-doped $TiO_2$ as a high-temperature $NO_2$ gas sensor (Gönüllü et al., 2015). Wang et al. demonstrated that the response value of $Cr_2O_3$/ZnO nanofibers was 3.6 to 1 ppm ethanol vapor at 300°C (Wang et al., 2010). Park et al. synthesized $In_2O_3$ nanorods decorated with $Cr_2O_3$-nanoparticles which showed excellent sensing properties to ethanol than other gases (Park et al., 2015). However, there are few reports on Synthesis of $Cr_2O_3$ nanoparticle-coated $SnO_2$ nanofibers and its $C_2H_2$ sensing properties.

In the paper, we reported the synthesis of $Cr_2O_3$ nanoparticle-coated $SnO_2$ nanofibers ($Cr_2O_3$ NPs. coated $SnO_2$ NFs.) by a sol–gel method and electrospinning technique. The prepared $Cr_2O_3$ NPs. coated $SnO_2$ NFs. were characterized by X-ray diffraction (XRD), scanning electron microscope (SEM), X-ray energy dispersive spectroscopy (EDS), X-ray photoelectron spectroscopy (XPS) and their $C_2H_2$ sensing properties were studied. Benefiting from the coating of $Cr_2O_3$, the $SnO_2$ nanofibers exhibited good sensitivity to $C_2H_2$ gas. In addition, a plausible gas sensing mechanism was proposed which may enhance the gas sensing performances of $C_2H_2$.

## EXPERIMENTAL DESIGN, MATERIALS, AND METHODS

### Sample Synthesis

$Cr_2O_3$ nanoparticles (NPs.) were prepared by a sol-gel method (Puerari et al., 2016). Firstly, 5.0g $Cr(NO_3)_3.9H_2O$ and 1.5 g NaOH were added to 100 ml distilled water for 30 min with stirring to obtain the precursor $Cr(OH)_3$. The $Cr(OH)_3$ was centrifuged at 5,000 rpm and washed several times with distilled water. It was then dried in an oven at 90*C* for 24 h. 0.05 g of $Cr(OH)_3$ powders were mixed with 10 g of deionized water and heated to 60°C and then stirred for 2 h to obtain a homogeneous sol solution.

$SnO_2$ nanofibers (NFs.) were synthesized by electrospinning method (Yang et al., 2018). Firstly, 6 mL N, N-dimethylformamide (DMF) and 1.2 g $SnCl_2 2H_2O$ were put into beaker1 and stirred for 2 h with a magnetic stirrer until it became a clarifying solution and set aside. 1 g PVP and 6 mL absolute ethanol were put in beaker2 and stirred with magnetic stirrer at uniform speed until PVP dissolved completely. The solution in beaker2 was added to the solution in beaker1 drop by drop with dropper, and the mixture was obtained as the precursor solution by stirring for 3 h at room temperature. The obtained spinning solution was conveyed to a hypodermic syringe at a constant flow rate, and then 20 kV voltage was applied to electrospinning at the electrode distance of 25 cm. A piece of aluminum foil was used as the cathode, and several sensor substrates were placed on it. Sensor substrates were prepared on $SiO_2$/Si chips by radio frequency sputtering platinum arrays as signal electrodes (Qi et al., 2014). The thickness of the $SiO_2$ layer and the platinum array are about 300 and 100 nm, respectively. The precursor solution was directly electrospun on sensor substrates with arrays of interdigitated platinum electrodes. After 2 h of electrospinning, the substrates were calcined in air at 500°C for 2 h, and then impregnated with the sol solution. The substrates were dried on a gently heated hot plate before the next

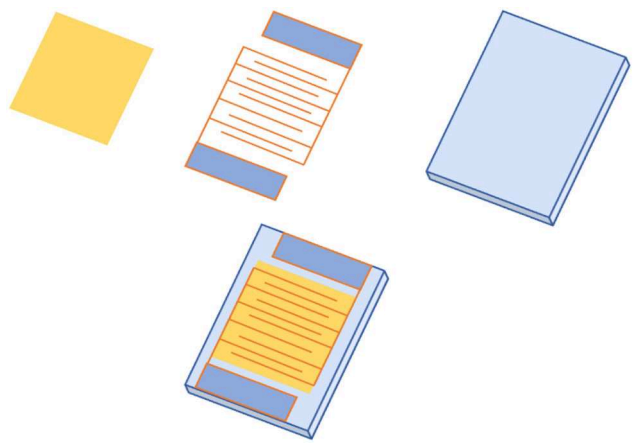

**FIGURE 1 |** The structure of the planar gas sensor.

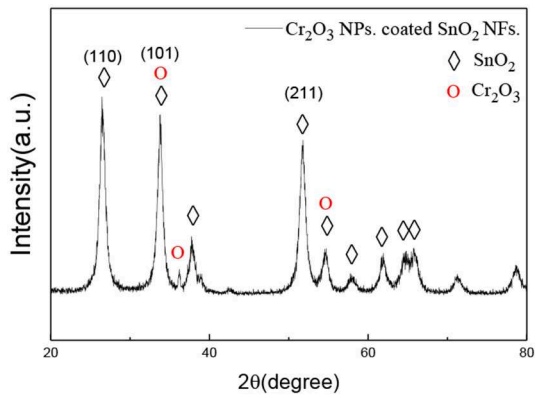


**FIGURE 2 |** The XRD spectrum of $Cr_2O_3$ NPs. coated $SnO_2$ NFs.

step after each step. Subsequently, the sensors were calcined in air at 600°C for 1 h, and then annealed in hydrogen atmosphere at 300°C for 10 min. Finally, the $Cr_2O_3$ NPs. coated $SnO_2$ NFs. sensors were obtained.

## Sample Characterization

In this paper, The X-ray diffractometer (D/Max-1200, Rigaku, Japan) was used to recorded XRD patterns at room temperature. The SEM and EDS images were gained by using Field Emission Electron Microscope (Hitachi S-4800, Marco Polo Shanghai Yongming Automation Equipment Co., Ltd., Shanghai, China) and Oxford INCA 250 EDS detector (JSM-6700F, Japan), respectively. The XPS spectra were determined on an X-ray photoelectron spectrometer (KRATOS XSAM800, Kratos, Kingdom).

The gas sensing properties of the obtained $Cr_2O_3$ NPs. coated $SnO_2$ NFs. were performed with the CGS-1TP intelligent gas sensitive analysis system (Beijing Elite Tech Co., Ltd, Beijing, China). The structure of planar gas sensor was shown in **Figure 1**. The gas sensing experiments were tested under laboratory conditions at the room temperature of 25°C and relative humidity of 50%. The gas response of the sensor (R) is defined as $R = R_g/R_a$ (Du et al., 2018), where $R_g$ and $R_a$ are the resistance values of the sensor in the air and the gas to be measured, respectively. The time required for the sensor resistance to change from $R_a$ to $R_a$-90% × ($R_a$-$R_g$) is defined as the response time when the target gas is introduced into the sensor, and the time from $R_g$ to $R_g$+90% × ($R_a$-$R_g$) is defined as recovery time when the target gas is replaced by air (Choi et al., 2019).

# RESULTS

## Materials Characterization

**Figure 2** demonstrated the XRD patterns of the prepared $SnO_2$ nanofiber sample with $Cr_2O_3$. The prominent peaks corresponding to (110), (101), and (211) crystal lattice planes and

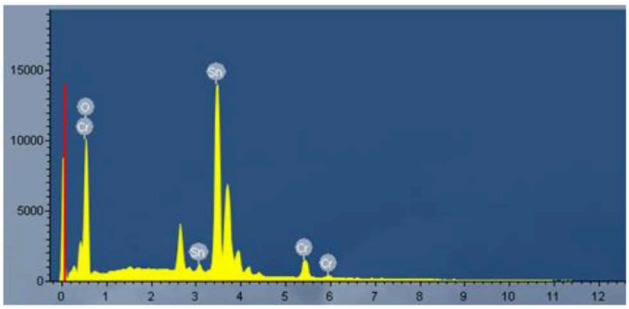


**FIGURE 5 |** The EDS spectrum of $Cr_2O_3$ NPs. coated $SnO_2$ NFs.

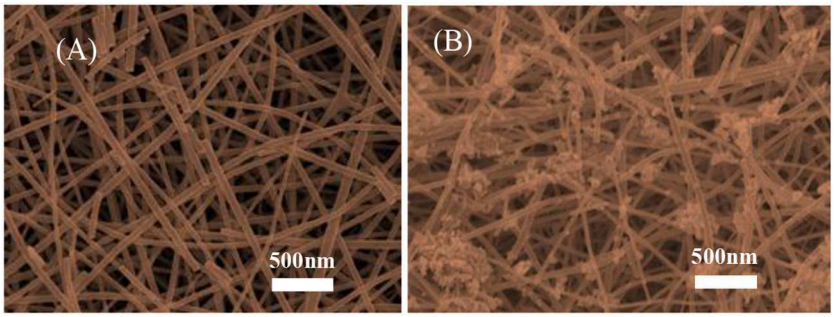


**FIGURE 3 |** The SEM images of **(A)** pure $SnO_2$ NFs. and **(B)** $Cr_2O_3$ NPs. coated $SnO_2$ NFs.

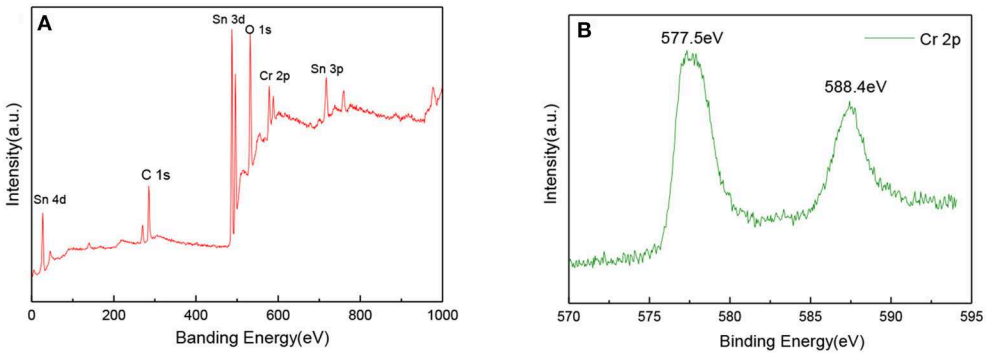


**FIGURE 4 | (A)** The XPS spectrum of the $Cr_2O_3$ NPs. coated $SnO_2$ NFs. sample, and **(B)** XPS spectrum of Cr 2p.

other smaller peaks showed no difference from the corresponding peaks of the $SnO_2$ rutile structure given in the standard data file (JCPDS File no. 41-1445). The diffraction peaks were observed at 34.7°, 37.8°, 54.2°, where the inconspicuous $Cr_2O_3$ peaks were observed, indicating that $Cr_2O_3$ successfully coated the $SnO_2$ sample.

The morphologies of the pure $SnO_2$ and $Cr_2O_3$ NPs. coated $SnO_2$ NFs. were examined by SEM and the representative images are shown in **Figure 3**. The prepared samples were composed of a plurality of $SnO_2$ nanofibers as shown in **Figure 3A**. The $SnO_2$ nanofibers were uniform in size and irregular arranged. After the synthesis process, the $Cr_2O_3$ nanoparticles were tightly coated on the surface of $SnO_2$ nanofibers. The surface of the nanofibers was uneven, long and continuous, without adhesion, intertwined into a network. Furthermore, it was observed from the photomicrograph that the prepared fibrous $SnO_2$ samples had a porous structure which was of benefit to subsequent gas sensitivity testing.

XPS is a kind of useful technique for studying the chemical state of the elements and the surface composition in the sample. **Figure 4A** showed the XPS spectrum of the $Cr_2O_3$ NPs. coated $SnO_2$ NFs. gas sensing material, and the chemical states of various elements in the sample were obtained. The C, Sn, Cr, and O elements appeared in the broad spectrum of the sample. The characteristic energy spectrum reflected that the Cr element had been successfully coated on the surface of $SnO_2$, which was consistent with the XRD pattern. At the same time, there was no impurity doping into $SnO_2$. **Figure 4B** showed the XPS spectrum of Cr 2p. The doublet peaks located at binding energies of 577.5 and 588.4 eV, which is close to the trivalent Cr ion in the standard XPS data, indicating Cr element was in the state of trivalent Cr ions.

An EDS measurement was performed to study the component of the sample. Corresponding EDS spectra from the prepared $Cr_2O_3$ NPs. coated $SnO_2$ NFs. sample is shown in **Figure 5**, which confirmed the presence of Sn, Cr, O, in the sample. So, it showed that the sample was composed of $Cr_2O_3$ and $SnO_2$ clearly.

## Sensing Performances

In order to find out whether the coating of $Cr_2O_3$ has a positive effect on the detection of acetylene gas by pure $SnO_2$, the gas sensing properties of pure $SnO_2$ and $Cr_2O_3$ NPs. coated $SnO_2$ NFs. for $C_2H_2$ gas were tested. As we know, the operating temperature is one of important factors that determine the gas sensitivity of materials. **Figure 6A** shows the response of pure

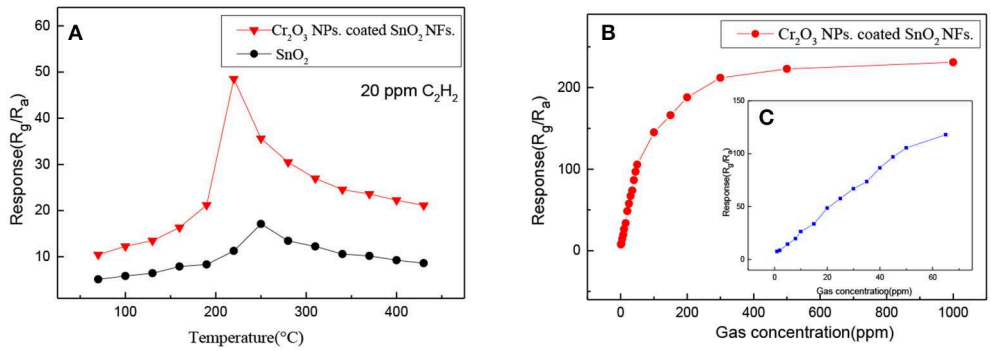


**FIGURE 6 | (A)** The gas response of the pure $SnO_2$ and $Cr_2O_3$ NPs. coated $SnO_2$ NFs. toward 20 ppm of $C_2H_2$ at different working temperatures (60–440°C); **(B)** the gas response of the $Cr_2O_3$ NPs. coated $SnO_2$ NFs. to different concentrations (0–1,000 ppm) $C_2H_2$ at 220°C and **(C)** the gas response of the $Cr_2O_3$ NPs. coated $SnO_2$ NFs. in the range from 0 to 80 ppm $C_2H_2$ at 220°C.

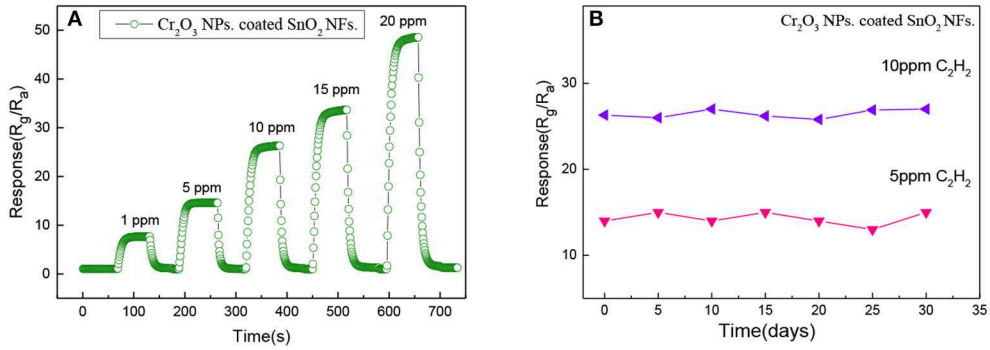


**FIGURE 7 | (A)** The dynamic response-recovery characteristic of $Cr_2O_3$ NPs. coated $SnO_2$ NFs. sample at different concentrations (1, 5, 10, 15, 20 ppm) at optimal operating temperature and **(B)** the long-term stability of $Cr_2O_3$ NPs. coated $SnO_2$ NFs to 5 and 10 ppm $C_2H_2$ at 220°C.

$SnO_2$ and $Cr_2O_3$ NPs. coated $SnO_2$ NFs. to 20 ppm $C_2H_2$ at different temperatures to explore the relationship between temperature and gas response as well as the optimal operating temperature in the range of 60–440°C. It found that the response of the samples showed the trend of increasing first and then decreasing. The response increased in the range of 60–250°C and reached the highest point at 250°C then decreased in the range of 250–440°C for pure $SnO_2$. The response increased in the range of 60–220°C and reached the highest point at 220°C then decreased in the range of 220–440°C for $Cr_2O_3$ NPs. coated $SnO_2$ NFs. The response values of gas sensor based on pure $SnO_2$ and $Cr_2O_3$ NPs. coated $SnO_2$ NFs. for 20 ppm $C_2H_2$ gas at optimum operating temperature were 17.12 and 48.54, respectively. Obviously, $Cr_2O_3$ NPs. coated $SnO_2$ NFs. exhibited excellent temperature characteristics with the lower optimal operating temperature and higher response value, indicating that the coating of $Cr_2O_3$ had a positive effect on the measurement of $C_2H_2$, and the optimum operating temperature was effectively reduced.

**Figure 6B** revealed the response of $Cr_2O_3$ NPs. coated $SnO_2$ NFs. to the concentrations of $C_2H_2$ in the range of 0 to 1,000 ppm at 220°C. The measured results in **Figure 6C** showed that the gas responses of $Cr_2O_3$ NPs. coated $SnO_2$ NFs. increased in a good linear relationship with the concentrations of $C_2H_2$ in the range from 0 to 60 ppm. Moreover, when the gas concentrations exceeded 200 ppm, the response increased slowly, indicating that the response gradually became saturated.

Quick response and recovery plays an important role for a gas sensing material. The dynamic response-recovery curve of the $Cr_2O_3$ NPs. coated $SnO_2$ NFs. sensors for 1, 5, 10, 15, and 20 ppm

**TABLE 1 |** The gas-sensing characteristics of $C_2H_2$ sensors based on different metal oxides synthesized by various methods.

| Materials | Method | Temperature (°C) | Concentrations | Response | Selectivity | Reference |
|---|---|---|---|---|---|---|
| $WO_3$ | Hydrothermal | 275 | 200 (ppm) | 32.31 | – | Wei et al., 2019a |
| Au-ZnO/$In_2O_3$ | Chemical vapor deposition process | 90 | 500 (ppm) | 13 | $C_2H_2$ >CO,$CH_4$, $C_3H_8$,$C_2H_5OH$ | Wang et al., 2017a |
| ZnO/$In_2O_3$ | Chemical vapor deposition process | 90 | 500 (ppm) | 2.9 | $C_2H_2$ >CO,$CH_4$, $C_3H_8$,$C_2H_5OH$ | |
| ZnO | Plasma immersion ion implantation and deposition | 280 | 1 vol% | – | $C_2H_2$ >$CO_2$,$CH_4$ | Oliveira et al., 2019 |
| $Fe_2O_3$-$SnO_2$ NPs. | Flame-spray-made | 300 | 3 vol% | – | $C_2H_2$ >$NO_2$,NO, $CO_2$,$C_2H_5OH$ | Sukunta et al., in press |
| $SmFeO_3$ | Polymer Precursor Method | 400 | 5 (ppm) | 18 | – | Tasaki et al., 2019 |
| $Cr_2O_3$ NPs. coated $SnO_2$ NFs. | Sol–gel method and electrospinning | 220 | 20 (ppm) | 48.54 | – | This work |

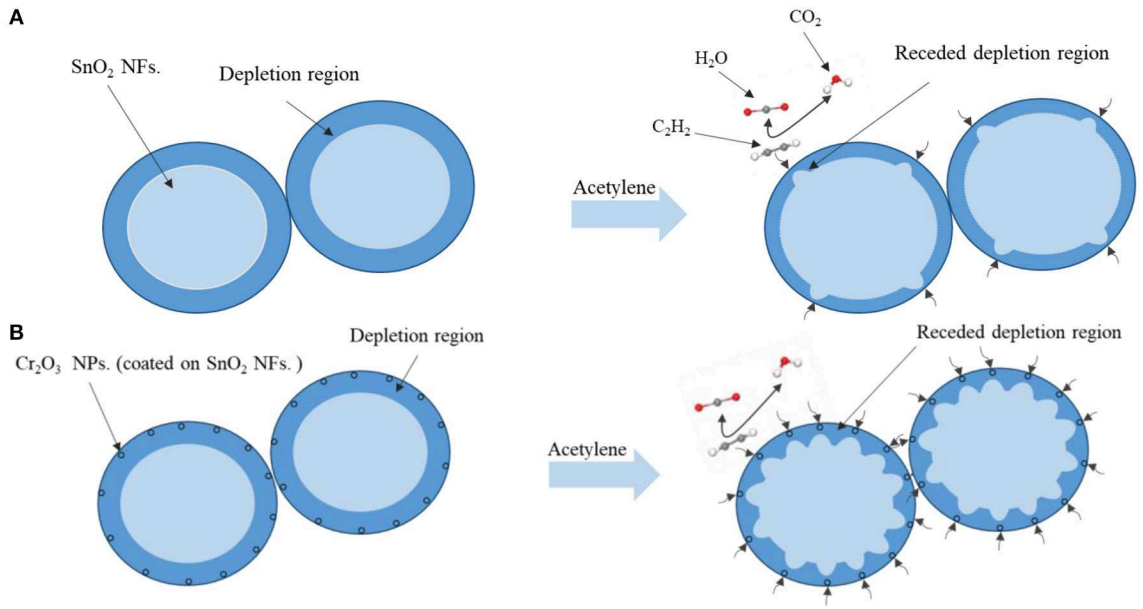


**FIGURE 8 |** The mechanism diagram of $C_2H_2$ sensing process of **(A)** pure $SnO_2$ and **(B)** $Cr_2O_3$ nanoparticle-coated $SnO_2$ nanofibers.

$C_2H_2$ gas at an optimum operating temperature of 220°C was tested and shown in **Figure 7A**. When the $C_2H_2$ concentration was increased from 1 to 20 ppm, the response time values of the prepared gas sensor were 9, 12, 15, 17, and 20 s, and the recovery time values were 11, 14, 18, 19, and 23 s. The $Cr_2O_3$ NPs. coated $SnO_2$ NFs. responded rapidly and could recover to its initial value when they were exposed to the air again. It showed that the sensors had good response recovery characteristics for different concentrations of $C_2H_2$ gas, indicating an excellent persistence and stability of $C_2H_2$ gas.

For the long-term perspective of practicality, in order to ensure the correctness of the test results, gas sensing materials should keep good stability. Therefore, the long-term stability of $Cr_2O_3$ NPs. coated $SnO_2$ NFs. to 5 and 10 ppm $C_2H_2$ were tested at 220°C during 30 days to ensure the reliability, as shown in **Figure 7B**. Even if the response values changed every day, when the gas concentrations were 5 and 10 ppm, the response values only just fluctuated around 14.5 and 26.5, respectively. So, the $Cr_2O_3$ NPs. coated $SnO_2$ NFs. had prominent stability.

The gas-sensing characteristics of $C_2H_2$ based sensors have been discussed and compared with other metal oxides material gas sensors shown in **Table 1**. From these reports, gas sensors based on $Cr_2O_3$ NPs. coated $SnO_2$ NFs. exhibit lower working temperatures and higher response values compared with most other sensors for $C_2H_2$ gas. The obtained results indicate that the $Cr_2O_3$ NPs. coated $SnO_2$ NFs sensor is promising for $C_2H_2$ gas sensing.

$SnO_2$ is a wide-bandgap semiconductor whose gas-sensing properties is the change in resistance caused by the adsorption and desorption of surface electrons and gas molecules. The gas sensing mechanism of pure $SnO_2$ NFs. and $Cr_2O_3$ NPs. coated $SnO_2$ NFs. was shown in **Figure 8**. When the sample exposed to the air, the resistant of the sensor was decided by the quantity of chemisorbed oxygen species. In the air, the oxygen would be chemically adsorbed on the surface of $SnO_2$ and electrons were obtained from conduction band of $SnO_2$, leading to the formation of ionic species such as $O^-$, $O^{2-}$, and $O_2^-$. When the $SnO_2$ NFs. was exposed to the atmosphere of $C_2H_2$, $C_2H_2$ gas had many opportunities for absorption and desorption on the surface. Reactions could be induced after coming into contact with acetylene molecules and then being oxidized with ionic oxygen species to produce $H_2O$ and $CO_2$. Thus, the desorbed oxygen species would set free electrons return into the conduction band of $SnO_2$, causing a receded depletion zone, decreasing the resistance, and increasing conductivity shown in **Figure 8A**.

It is well-known that the ability of chemisorbed oxygen is decided by the specific surface area of the materials and the operating temperature. The surface area of $Cr_2O_3$ NPs. coated $SnO_2$ NFs. was large, as shown in **Figure 3**, which indicated that the adsorption capability of $Cr_2O_3$ NPs. coated $SnO_2$ NFs. had been enormously enhanced. $Cr_2O_3$ coating provided an effective means with improving the electronic and catalytic properties for gas interaction at the interface. The concentration of oxygen vacancies was greatly increased. The oxygen vacancies could capture ion-adsorbed oxygen in the atmosphere, which facilitated gas sensing reaction. Meanwhile, $Cr_2O_3$ coating increased the specific surface area, provided more gas and oxygen adsorption sites, improved the conductivity of $SnO_2$, and contributed to oxygen adsorption (Li et al., 2018; Zhou et al., 2018a) as shown in **Figure 8B**. Accordingly, the speed at which the reaction occured was accelerated. The adsorption rate of $C_2H_2$ to $SnO_2$ increased with $Cr_2O_3$ coating, which indicated that $Cr_2O_3$ could improve the sensitivity of $SnO_2$ to $C_2H_2$ gas.

## CONCLUSIONS

The $Cr_2O_3$ NPs. coated $SnO_2$ NFs. were successfully prepared via a sol-gel process and electrospinning method. The gas detection results showed that the prepared sensor was sensitive to $C_2H_2$, and the optimum temperature was about 220°C which was lower than the optimum temperature of pure $SnO_2$ nanofibers. $C_2H_2$ gas had a higher response value, and the $C_2H_2$ concentration had a good linear relationship with the response value when the concentration was <60 ppm. Moreover, the $Cr_2O_3$ NPs. coated $SnO_2$ NFs. had good repeatability and long-term stability. The excellent gas sensing performance of $Cr_2O_3$ NPs. coated $SnO_2$ NFs. could be owing to the increase of oxygen vacancies of $SnO_2$ nanofibers by $Cr_2O_3$ coating and the large specific surface of the sample. The results certify that the $Cr_2O_3$ NPs. coated $SnO_2$ NFs. material is a potential candidate for the detection of acetylene.

## DATA AVAILABILITY

All datasets generated for this study are included in the manuscript/supplementary files.

## AUTHOR CONTRIBUTIONS

XG and ZL performed the experiments and analyzed the data with the help from LX and QiZ. XG, QuZ, and WZ wrote and revised the manuscript with input from all authors. All authors read and approved the manuscript.

## ACKNOWLEDGMENTS

This work has been supported in part by the National Natural Science Foundation of China (No. 51507144), Fundamental Research Funds for the Central Universities (No. XDJK2019B021), the artificial intelligence key project of Chongqing (No. cstc2017rgzn-zdyfX0030), the Chongqing Science and Technology Commission (CSTC) (No. cstc2016jcyjA0400), and the project of China Scholarship Council (CSC).

## REFERENCES


Ahmed, A., Siddique, M. N., Ali, T., and Tripathi, P. (2019). Defect assisted improved room temperature ferromagnetism in Ce doped $SnO_2$ nanoparticles. *Appl. Surf. Sci.* 483, 463–471. doi: 10.1016/j.apsusc.2019.03.209

Bai, S. L., Fu, H., Zhao, Y. Y., Tian, K., and Chen, A. F. (2018). On the construction of hollow nanofibers of ZnO-$SnO_2$ heterojunctions to enhance the $NO_2$ sensing properties. *Sens. Actuators B* 266, 692–702. doi: 10.1016/j.snb.2018.03.055

Chang, L. M., Yi, Z., Wang, Z. M., Wang, L. M., and Cheng, Y. (2019). Ultrathin $SnO_2$ nanosheets anchored on graphene with improved electrochemical kinetics for reversible lithium and sodium storage. *Appl. Surf. Sci.* 484, 646–654. doi: 10.1016/j.apsusc.2019.04.144

Choi, M. S., Mirzaei, A., Bang, J. H., Oum, W., Kwon, Y. J., Kim, J.-H., et al. (2019). Selective $H_2S$-sensing performance of Si nanowires through the formation of ZnO shells with Au functionalization. *Sens. Actuators B Chem.* 289, 1–14. doi: 10.1016/j.snb.2019.03.047

Crişan, M., Mardare, D., Ianculescu, A., Drăgan, N., and Vasile, B. (2018). Iron doped $TiO_2$ films and their photoactivity in nitrobenzene removal from water. *Appl. Surf. Sci.* 455, 201–215. doi: 10.1016/j.apsusc.2018.05.124

Du, Q., Wang, L., Yang, J., Liu, J. F., Yuan, Y. K., Wang, M. Z., et al. (2018). Enhancing gas sensing performances and sensing mechanism at atomic and molecule level of $WO_3$ nanoparticles by hydrogenation. *Sens. Actuators B Chem.* 273, 1786–1793. doi: 10.1016/j.snb.2018.07.099

Gönüllü, Y., Haidry, A. A., and Saruhan, B. (2015). Nanotubular Cr-doped $TiO_2$ for use as high-temperature $NO_2$ gas sensor, Sens. *Actuators B Chem.* 217, 78–87. doi: 10.1016/j.snb.2014.11.065

Inyawilert, K., Wisitsoraat, A., Liewhiran, C., Tuantranont, A., and Phanichphant, S. (2019). $H_2$ gas sensor based on $PdO_x$-doped $In_2O_3$ nanoparticles synthesized by flame spray pyrolysis. *Appl. Surf. Sci.* 475, 191–203. doi: 10.1016/j.apsusc.2018.12.274

Li, F., Ruan, S. P., Zhang, N., Yin, Y. Y., Guo, S. J., Chen, Y., et al. (2018). Synthesis and characterization of Cr-doped $WO_3$ nanofibers for conductometric sensors with high xylene sensitivity. *Sens. Actuators B Chem.* 265, 355–364. doi: 10.1016/j.snb.2018.03.054

Li, H., Zhang, B., Wang, X., Zhang, J., An, T. H., Ding, Z. Y., et al. (2019a). Heterostructured $SnO_2$-$SnS_2$@C embedded in nitrogen-doped graphene as a robust anode material for lithium-ion batteries. *Front. Chem.* 7:339. doi: 10.3389/fchem.2019.00339

Li, Z. Y., Yang, Q. B., Wu, Y. P., He, Y., and Wang, J. F. (2019b). $La^{3+}$ doped $SnO_2$ nanofibers for rapid and selective $H_2$ sensor with long range linearity. *Int. J. Hydrogen Energy* 44, 8659–8668. doi: 10.1016/j.ijhydene.2019.02.050

Liu, X. J., Tian, X. Y., Jiang, X. M., Jiang, L., and Xu, X. J. (2018). Facile preparation of hierarchical Sb-doped $In_2O_3$ microstructures for acetone detection. *Sens. Actuators B Chem.* 270, 304–311. doi: 10.1016/j.snb.2018.05.046

Lu, Z., Zhou, Q., Wang, C., Wei, Z., Xu, L., and Gui, Y. (2018). Electrospun ZnO–$SnO_2$ composite nanofibers and enhanced sensing properties to $SF_6$ decomposition byproduct $H_2S$. *Front. Chem.* 6:540. doi: 10.3389/fchem.2018.00540

Meng, L. J., Wang, Z. H., Yang, L., Ren, W. J., and Santos, M. P. (2019). A detailed study on the Fe-doped $TiO_2$ thin films induced by pulsed laser deposition route. *Appl. Surf. Sci.* 474, 211–217. doi: 10.1016/j.apsusc.2018.03.043

Mudra, E., Shepa, I., Milkovic, O., Dankova, Z., Kovalcikova, A., Annušová, A., et al. (2019). Effect of iron doping on the properties of $SnO_2$ nano/microfibers. *Appl. Surf. Sci.* 480, 876–881. doi: 10.1016/j.apsusc.2019.03.041

Oliveira, R. M., Vieira, M. S., and Silva, N. F. (2019). Enhancement of acetylene gas sensing properties for a ZnO-based gas sensor produced by plasma immersion ion implantation and deposition. *Mater. Sci. Semicond. Process.* 93, 339–344. doi: 10.1016/j.mssp.2018.12.031

Park, S., Kim, S., Sun, G.-J., Choi, S., Lee, S., and Lee, C. (2015). Ethanol sensing properties of networked $In_2O_3$ nanorods decorated with $Cr_2O_3$-nanoparticles. *Ceram. Int.* 41, 9823–9827. doi: 10.1016/j.ceramint.2015.04.055

Puerari, R. C., Costa, C. H., Vicentini, D. S., Fuzinatto, C. F., Melegari, S. P., Schmidt, É. C., et al. (2016). Synthesis, characterization and toxicological evaluation of $Cr_2O_3$ nanoparticles using *Daphnia magna* and *Aliivibrio fischeri*. *Ecotoxicol. Environ. Saf.* 128, 36–43. doi: 10.1016/j.ecoenv.2016.02.011

Qi, Q., Zhang, T., Zheng, X. J., Fan, H. T., and Zeng, Y. (2008). Electrical response of $Sm_2O_3$-doped $SnO_2$ to $C_2H_2$ and effect of humidity interference. *Sens. Actuators B Chem.* 134, 36–42. doi: 10.1016/j.snb.2008.04.011

Qi, Q., Zhao, J., Xuan, R. F., Wang, P. P., and Li, G. D. (2014). Sensitive ethanol sensors fabricated from p-type $La_{0.7}Sr_{0.3}FeO_3$ nanoparticles and n-type $SnO_2$ nanofibers. *Sens. Actuators B Chem.* 191, 659–665. doi: 10.1016/j.snb.2013.10.035

Ren, L., Yao, Y., Wang, K. Y., Li, S. T., Zhu, K. J., and Liu, J. (2019). Novel one-step in situ growth of $SnO_2$ quantum dots on reduced graphene oxide and its application for lithium ion batteries. *J. Solid State Chem.* 273, 128–131. doi: 10.1016/j.jssc.2019.01.028

Sukunta, J., Wisitsoraat, A., Tuantranont, A., Jaruwongrungsee, K., Phanichphant, S., and Liewhiran, C. (in press). Mechanistic roles of substitutional Fe dopants on catalytic acetylene-sensing process of flame-made $SnO_2$ nanoparticles. *Arab. J. Chem.* doi: 10.1016/j.arabjc.2018.08.013

Tasaki, T., Takase, S., and Shimizu, Y. (2019). Improvement of sensing performance of impedancemetric $C_2H_2$ sensor using $SmFeO_3$ thin-films prepared by a polymer precursor method. *Sensors* 19:E773. doi: 10.3390/s19040773

Thanihaichelvan, T., Thanihaichelvan, M., Haseeb, M., A. S. M. A., and Akbar, S. A. (2019). Highly sensitive and selective ethanol sensor based on ZnO nanorod on SnO2 thin film fabricated by spray pyrolysis. *Front. Chem.* 6:122. doi: 10.3389/fmats.2019.00122

Tonezzer, M. (2019). Selective gas sensor based on one single $SnO_2$ nanowire. *Sens. Actuators B Chem.* 288, 53–59. doi: 10.1016/j.snb.2019.02.096

Uddin, A. S. M. I., and Chung, G. S. (2015). Fabrication and characterization of $C_2H_2$ gas sensor based on Ag-loaded vertical ZnO nanowires array. *Proced. Eng.* 120, 582–585. doi: 10.1016/j.proeng.2015.08.730

Wang, B., Jin, H. T., Zheng, Z. Q., Zhou, Y. H., and Gao, C. (2017a). Low-temperature and highly sensitive $C_2H_2$ sensor based on Au decorated ZnO/$In_2O_3$ belt-tooth shape nano-heterostructures. *Sens. Actuators B Chem.* 244, 344–356. doi: 10.1016/j.snb.2016.12.044

Wang, D., Zhang, M. L., Chen, Z. L., Li, H. J., and Yang, J. H. (2017b). Enhanced formaldehyde sensing properties of hollow $SnO_2$ nanofibers by graphene oxide. *Sens. Actuators B Chem.* 250, 533–542. doi: 10.1016/j.snb.2017.04.164

Wang, J. X., Zhou, Q., and Zeng, W. (2019). Competitive adsorption of $SF_6$ decompositions on Ni-doped ZnO (100) surface: Computational and experimental study. *Appl. Surf. Sci.* 479, 185–197. doi: 10.1016/j.apsusc.2019.01.255

Wang, W., Li, Z. Y., Zheng, W., Huang, H. M., and Sun, J. H. (2010). $Cr_2O_3$-sensitized ZnO electrospun nanofibers based ethanol detectors. *Sens. Actuators B Chem.* 143, 754–758. doi: 10.1016/j.snb.2009.10.016

Wei, Z. J., Zhou, Q., Lu, Z. R., Xu, L. N., Gui, Y. G., and Tang, C. (2019a). Morphology controllable synthesis of hierarchical $WO_3$ nanostructures and $C_2H_2$ sensing properties. *Phys. E* 109, 253–260. doi: 10.1016/j.physe.2019.01.006

Wei, Z. J., Zhou, Q., Wang, J. X., Gui, Y. G., and Zeng, W. (2019b). A novel porous NiO nanosheet and its $H_2$ sensing performance. *Mater. Lett.* 245, 166–169. doi: 10.1016/j.matlet.2019.03.013

Yang, Y., Zhang, Z. J., He, Y. L., Wang, Z. H., Zhao, Y. B., and Sun, L. (2018). Fabrication of Ag@$TiO_2$ electrospinning nanofibrous felts as SERS substrate for direct and sensitive bacterial detection. *Sens. Actuators B Chem.* 273, 600–609. doi: 10.1016/j.snb.2018.05.129

Yoo, R., Güntner, A. T., Park, Y. J., Rim, H. J., Lee, H.-S., and Lee, W. (2019). Sensing of acetone by Al-doped ZnO. *Sens. Actuators B Chem.* 283, 107–115. doi: 10.1016/j.snb.2018.12.001

Zhang, Q., Zhou, Q., Lu, Z., Wei, Z., Xu, L., and Gui, Y. (2018). Recent advances of $SnO_2$-based sensors for detecting fault characteristic gases extracted from power transformer oil. *Front. Chem.* 6:364. doi: 10.3389/fchem.2018.00364

Zhang, Q. Y., Zhou, Q., Yin, X. T., Liu, H. C., Xu, L. N., Tan, W. M., et al. (2017). The effect of PMMA pore-forming on hydrogen sensing properties of porous $SnO_2$ thick film sensor. *Sci. Adv. Mater.* 9, 1350–1355. doi: 10.1166/sam.2017.3111

Zheng, Y. Q., Liu, J. Y., Cheng, B., You, W., Ho, W. K., and Tang, H. (2019). Hierarchical porous $Al_2O_3$@ZnO core-shell microfibres with excellent adsorption affinity for Congo red molecule. *Appl. Surf. Sci.* 473, 251–260. doi: 10.1016/j.apsusc.2018.12.106

Zhou, Q., Chen, W. G., Li, J., Tang, C., and Zhu, S. P. (2016). Synthesis, characterisation and sensing properties of $Sm_2O_3$ doped $SnO_2$ nanorods to

$C_2H_2$ gas extracted from power transformer oil. *Mater. Technol.* 31, 364–370. doi: 10.1179/1753555715Y.0000000069

Zhou, Q., Chen, W. G., Xu, L. N., Kumarc, R., Gu, Y. G., Zhao, Z. Y., et al. (2018a). Highly sensitive carbon monoxide (CO) gas sensors based on Ni and Zn doped $SnO_2$ nanomaterials. *Ceram. Int.* 44, 4392–4399. doi: 10.1016/j.ceramint.2017.12.038

Zhou, Q., Lu, Z., Wei, Z., Xu, L., and Gui, Y. (2018b). Hydrothermal synthesis of hierarchical ultrathin NiO nanoflakes for high-performance $CH_4$ sensing. *Front. Chem.* 6:194. doi: 10.3389/fchem.2018.00194

Zhou, Q., Umar, A., Sodki, E. M., Amine, A., Xu, L. N., Gui, Y. G., et al. (2018c). Fabrication and characterization of highly sensitive and selective sensors based on porous NiO nanodisks. *Sens. Actuators B Chem.* 259, 604–615. doi: 10.1016/j.snb.2017.12.050

Zhou, Q., Xu, L. N., Umar, A., Chen, W. G., and Kumr, R. (2018d). Pt nanoparticles decorated $SnO_2$ nanoneedles for efficient CO gas sensing applications. *Sens. Actuators B* 256, 656–664. doi: 10.1016/j.snb.2017.09.206

**Conflict of Interest Statement:** The authors declare that the research was conducted in the absence of any commercial or financial relationships that could be construed as a potential conflict of interest.